

# DEEP-LEARNING-BASED CHANGE DETECTION WITH SPACEBORNE HYPERSPECTRAL PRISMA DATA

*J.F. Amieva<sup>1\*</sup>, A. Austoni<sup>1\*</sup>, M.A. Brovelli<sup>1</sup>, L. Ansalone<sup>2</sup>, P. Naylor<sup>3</sup>, F. Serva<sup>2,3†</sup>, B. Le Saux<sup>3</sup>*

<sup>1</sup>Dipartimento di Ingegneria Civile e Ambientale,  
Politecnico di Milano, Milano I-20133, Italy

<sup>2</sup>Agenzia Spaziale Italiana, Via del Politecnico snc, Roma I-00133, Italy

<sup>3</sup>Φ-lab, ESRIN, European Space Agency, Frascati I-00044, Italy

## ABSTRACT

Change detection (CD) methods have been applied to optical data for decades, while the use of hyperspectral data with a fine spectral resolution has been rarely explored. CD is applied in several sectors, such as environmental monitoring and disaster management. Thanks to the PRekursore IperSpettrale della Missione operativa (PRISMA), hyperspectral-from-space CD is now possible. In this work, we apply standard and deep-learning (DL) CD methods to different targets, from natural to urban areas. We propose a pipeline starting from coregistration, followed by CD with a full-spectrum algorithm and by a DL network developed for optical data. We find that changes in vegetation and built environments are well captured. The spectral information is valuable to identify subtle changes and the DL methods are less affected by noise compared to the statistical method, but atmospheric effects and the lack of reliable ground truth represent a major challenge to hyperspectral CD.

**Index Terms**— Change detection, hyperspectral satellite, Earth observation

## 1. INTRODUCTION

Change detection (CD) is the set of procedures used to identify changes between multiple images, generally acquired at different times, which has been applied with success in remote sensing data for several decades [11]. It is also known that different CD methods can produce different change maps [16], and that often expert assessment is required to interpret and post-process results in a supervised fashion.

Deep learning (DL) methods have been gaining much attention as a tool for automatizing time-consuming CD tasks [7]. Since CD involves identifying spatial features and their changes between two different dates, convolutional neural networks (NNs) have proven to be highly successful for CD in optical and radar data [4, 8].

Unlike multispectral imagery, hyperspectral data provides very detailed information on the spectral characteristics of the sensed objects, allowing for example to discriminate between different materials or retrieve biogeophysical parameters accurately [13]. Historically, this kind of data has been collected from airborne platforms, while now multiple hyperspectral satellite missions are ongoing or planned, opening a new era for their applications.

PRISMA (PRekursore IperSpettrale della Missione operativa) is a mission of the Italian Space Agency (ASI) acquiring hyperspectral data globally since 2019. Further details on the mission are provided in Sec. 2. To our knowledge, CD with PRISMA have been limited so far, as recent works [1, 15] considered only individual pairs of images. In general, hyperspectral CD studies are challenged by the lack of suitable data, often restricted to a few regions of the world [10, 6, 17] or without temporality [5], with ground truth often unavailable for validation. Contributions of this work comprise 1) information on a list of PRISMA image pairs enabling change detection; 2) an assessment of unsupervised statistical and DL methods for CD with PRISMA data to illustrate their limits and potentialities.

## 2. DATA AND METHODS

### 2.1. PRISMA satellite data

The PRISMA mission was launched in June 2019 and is one of the latest imaging spectroscopy missions for Earth observation [9]. The PRISMA satellite has a hyperspectral imaging spectrometer (30 m GSD) and a panchromatic camera (5 m GSD). The hyperspectral sensor covers the visible and near-infrared (VNIR: 400 – 1010 nm, 66 bands) and the short-wave infrared (SWIR: 920 – 2505 nm, 174 bands) with a high spectral resolution, having a total of 240 bands. The acquisitions have a swath of 30 km with a revisit time below 29 days, and since they are primarily on-demand, based on requests by registered users, multitemporal and cloud-free images are not always available. However, the satellite has near-global acquisition capabilities, which provides potential coverage even

\*These authors contributed equally.

†Now at the National Research Council, Rome, Italy

**Table 1.** Details on the PRISMA acquisitions used.

Location	Dates	Lat/Lon (deg)
Athens	2020-07-22; 2022-07-05	37.94 / 23.95
Beirut	2020-08-23; 2022-06-26	33.86 / 35.55
Hanging Rock	2019-12-27; 2021-02-11	-31.49 / 151.29
Java	2021-04-21; 2021-07-17	-7.54 / 110.44
Lagos	2020-11-13; 2022-01-22	6.44 / 3.39
London	2020-06-24; 2022-07-18	51.48 / -0.46
Los Angeles	2020-07-21; 2022-07-16	34.01 / -118.22
Nalasopara	2019-12-31; 2022-02-21	19.47 / 72.84
Newark	2020-04-15; 2022-04-22	40.72 / -74.2
Rome	2020-08-06; 2022-06-15	41.86 / 12.26
Shanghai	2021-04-09; 2022-04-09	31.35 / 121.6

in remote areas. For this study, we use atmospheric-corrected and geocoded surface reflectance (L2D) data provided by ASI. An additional coregistration step is used to reduce shifts between images down to the pixel level.

Eleven pairs of PRISMA acquisitions with low cloud coverage are selected for our analysis. They are chosen to ensure global representativeness, sampling of different land cover states (e.g., rural, urban, or mixed), and consistent timing to reduce seasonal variations. Further information as acquisition times and coordinates is provided in Table 1.

## 2.2. Preprocessing and CD methods

PRISMA image pairs are **co-registered** with the *GeFolki* software [3], using the red band of PRISMA images, with similar results confirmed for other band selections. The ‘before’ (*b*) image is used as the target, and the ‘after’ (*a*) is the moving image. The optical flow derived with this method for the overlapping area is then used to correct all the bands of the moving image to better match the target, generally resulting in shifts below 5 pixels for complex terrains. Finally, square patches with size  $512 \times 512$  for the area of interest (AOI) are extracted and used to derive binary CD maps (Fig. 1).

Compressed **change vector analysis** (C2VA) is an unsupervised method [2] that fully exploits multispectral image information. Similar to the standard CVA [11], for each pixel a change magnitude ( $\rho$ ) and phase angle ( $\theta$ ) are calculated for the before and after images for  $B$  spectral bands, as  $\rho = \sqrt{\sum_{k=1}^B (X_{k,a} - X_{k,b})^2}$ . The phase angle is estimated from an arbitrary reference vector, e.g.  $X_{ref} = (\sqrt{B}/B, \dots, \sqrt{B}/B)$ , and can be used to identify coherent changes. Examples of magnitude and phase angle from C2VA for one scene are reported in Fig. 2. Notably changes in agricultural fields (upper left areas) or the mining area on the right have a similar phase, suggesting their common nature. For this work we focus on the magnitude information, making binary change maps based on a 90<sup>th</sup> percentile threshold calculated for each pair.

**DeepCVA** (DCVA) [14] is a method for generating a pixel

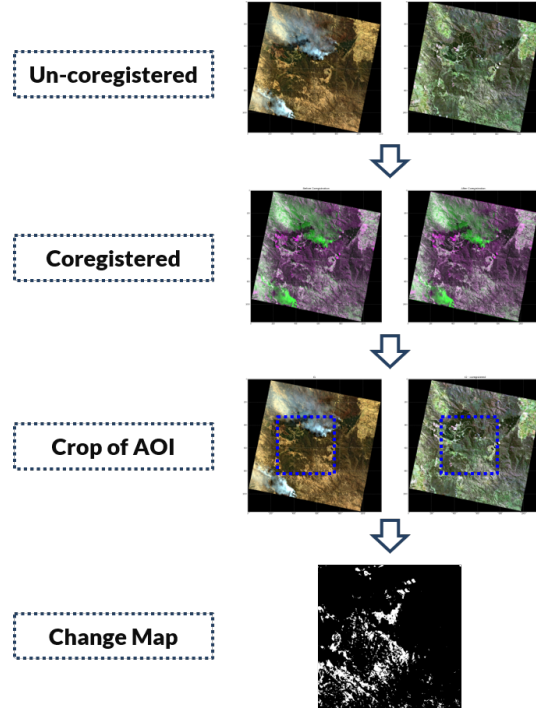


**Fig. 1.** Processing workflow example: RGB images and AOI (blue) (rows 1-3), CD map (row 4 - white: change, black: no change). Data processed under license (©ASI).

wise hyper vector  $G$  from the difference of a chosen subset of layers  $L$  from a pre-trained deep NN and performing unsupervised CD. The chosen subset is given apriori and is denoted by  $L \subset [1 : N]$  where  $N$  is the number of layers. We denote by  $F$  the NN composed of layers  $F^l$  with  $l \in [1 : N]$ . To simplify the notation, we denote by  $F_i^l$  the feature layer of  $X_i$  at layer  $F^l$  with  $i \in \{a, b\}$ .  $G$  is generated from the difference of extracted deep representations. In particular, we compute the difference for each given feature-layer  $l \in L$ :  $\delta_l = F_b^l - F_a^l$  and concatenate each  $\delta_l$  to obtain  $G$ . To limit the size of  $G$ , we refine the number of selected features at each layer of  $L$  by only retaining a certain percentile of features from  $\delta_l$ . For each layer  $l$ , we perform a pixel-wise spatial clustering and keep for each cluster the features with the highest variance within the top percentile. CD is then computed at a pixel-wise level, where a change is reported if  $\|G\| > \mathcal{T}$  where  $\mathcal{T}$  is a given threshold. For the computation of  $\mathcal{T}$ , we use a local adaptive thresholding method (DCVA Ada) or Otsu’s method (DCVA Otsu). We use a network pre-trained [14] on visible/infrared bands (RGBIR).

## 3. RESULTS AND DISCUSSION

An overview of CD results for all the pairs of PRISMA acquisitions is provided in Table 2, comparing different scenes and methods. By construction, 10% of the image is marked

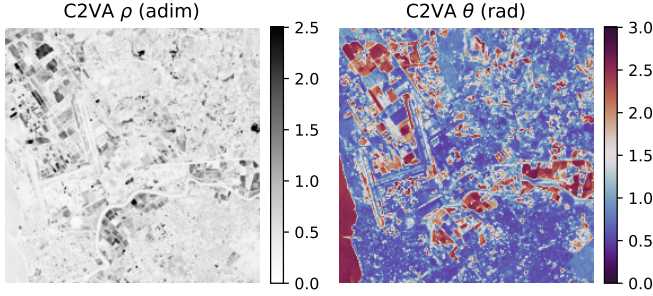


**Fig. 2.** Illustration of C2VA magnitude and angle obtained for the Rome image pair. Data processed under license (©ASI).

**Table 2.** Number of changed pixels (in %). (i) indicates the number of layers. (1) is layers [2, 5], (2) is [2, 5, 8, 10] and (3) is [2, 5, 8, 10, 11, 23]. DCVA Otsu is with (2).

Location	Type	C2VA	DCVA Otsu	DCVA Ada		
				(1)	(2)	(3)
Athens	urban	10	37.4	0.0	0.1	0.3
Beirut	mix	10	49.4	0.8	2.8	3.0
Hanging Rock	rural	10	39.4	0.6	1.5	1.1
Java	rural	10	22.0	0.7	2.7	2.7
Lagos	urban	10	4.2	2.2	2.6	2.3
London	urban	10	23.4	3.2	4.7	4.9
Los Angeles	urban	10	34.3	0.1	0.1	0.0
Nalasopara	rural	10	29.4	2.7	4.8	4.5
Newark	urban	10	16.6	2.1	2.7	3.4
Rome	mix	10	26.4	5.0	3.9	3.7
Shanghai	urban	10	37.0	2.0	2.3	1.6

as change for C2VA. DCVA with Otsu thresholding method is prone to overestimating the amount of changes. This is likely due to the fact that the difference histograms produced are not bimodal and therefore binarization is affected by noise or equalization issues (e.g., due to clouds). The estimates of DCVA Ada methods are much more conservative, with little or no change detected for urban scenes, such as Athens or Los Angeles. It should be noted that the network was pre-trained on high-resolution optical imagery, and the coarse spatial resolution of PRISMA may not be fully suitable for the task. The amount of changes identified by the network is not trivially related to the number of layers selected. For example in the Beirut scene, increasing the number of layers induces more detected changes, but fewer changes for the Shanghai pair. Moreover, in the case of Lagos, the presence of haze or smog in one image (not shown) leads to the smallest amount of changes detected overall. To visualize the contrast between the different methods and sensitivity to hyperparameters, we report a comparison of CD masks and corresponding RGB images in Fig. 3 and 4. These images illustrate how DCVA Otsu tends to mark water surfaces as changed, likely due to their different optical characteristics. Detected changes by the adaptive methods are a subset of Otsu’s method, and more

changes are picked up when more layers are considered. This may be explained by noting that a small number of layers is more suitable for homogeneous scenes. For the Beirut scene, in the most conservative setting (layer 2,5), changes are detected in the city centre, near the August 2020 explosion site. An interesting feature in Fig. 3 is that C2VA can identify ships in the upper right portion of the image, while they are missing when the change is identified in the latent space. For specific applications, such as ship detection, it would be important to tune the algorithms with real data as fine-grained details can be missing in the latent space. Large-scale land-use changes are however identified by both methods. In general, changes identified by C2VA appear noisy in urban scenes but are fairly consistent when their extent is larger, without the sensitivity of the DCVA Otsu for water bodies. In the absence of reliable ground-truth data, it is however hard to judge which method is performing better.

#### 4. CONCLUSIONS AND PERSPECTIVES

In this work, we present a comparison of statistical and DL methods for performing change detection on novel hyperspectral satellite data (from PRISMA). This is the first study to address hyperspectral-from-space with deep learning on a varied portfolio of changes, as operational hyperspectral satellite missions have only recently been launched. For this task, we selected eleven pairs of acquisitions. The areas were selected to represent the heterogeneity commonly found in EO data, including areas with clouds or ship traffic.

We find that larger scale changes in natural and urban scenes are successfully identified by the proposed methods. Sensitivity to terrain conditions and atmospheric effects is also noted. The moderate spatial resolution of PRISMA complicates the application of a pre-trained network using only four bands. In this case, results are very sensitive to the number of layers adopted. Training from scratch with a larger multispectral dataset would likely improve results.

Our work shows the potential of hyperspectral data for CD tasks. The lack of reliable ground truth data complicates the assessment of the different methods, but subjective evaluation indicates that the use of threshold-based methods is not always successful. The availability of datasets with high-quality ground truth labels would be useful for many applications, including the development of DL models and for semantic CD. We aim to release a public dataset for this purpose, as this is now possible thanks to current and new missions such as CHIME [12].

#### REFERENCES

- [1] S. Arjasakusuma et al. Change Detection Analysis using Bitemporal PRISMA Hyperspectral Data: Case Study of Magelang and Boyolali Districts, Central Java Province, In-



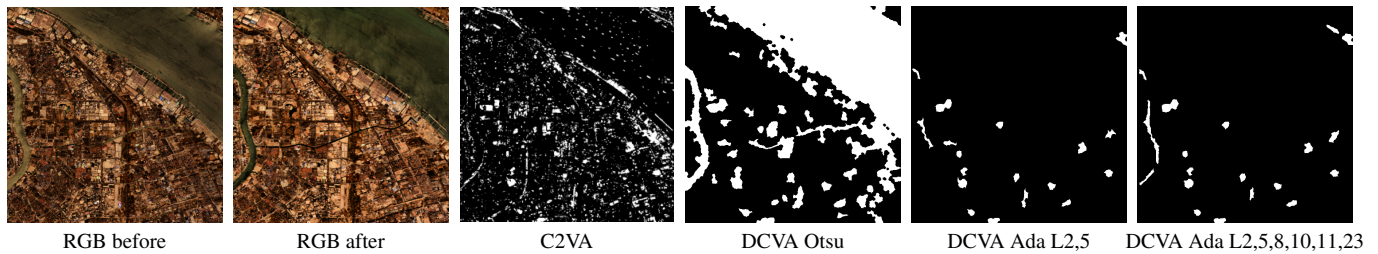


**Fig. 3.** Image pair for the Shanghai scene and change maps by different methods. Data processed under license (©ASI).

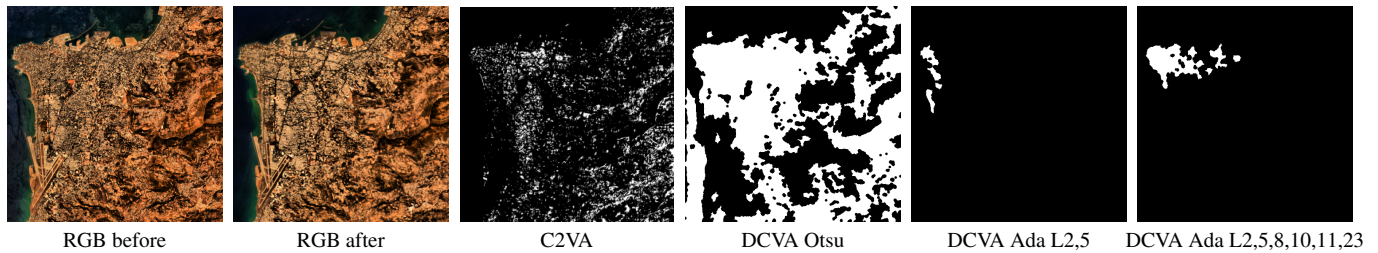


**Fig. 4.** As in Fig. 3, but for Beirut.

- donesia. *J. Ind. Soc. Rem. Sens.*, 2022. doi: [10.1007/s12524-022-01566-z](https://doi.org/10.1007/s12524-022-01566-z).
- [2] F. Bovolo, S. Marchesi, and L. Bruzzone. A Framework for Automatic and Unsupervised Detection of Multiple Changes in Multitemporal Images. *IEEE TGRS*, 50(6):2196–2212, 2012. doi: [10.1109/TGRS.2011.2171493](https://doi.org/10.1109/TGRS.2011.2171493).
- [3] G. Brigot et al. Adaptation and Evaluation of an Optical Flow Method Applied to Coregistration of Forest Remote Sensing Images. *IEEE JSTARS*, 9(7):2923–2939, 2016. doi: [10.1109/JSTARS.2016.2578362](https://doi.org/10.1109/JSTARS.2016.2578362).
- [4] R. Caye Daudt et al. Urban change detection for multispectral earth observation using convolutional neural networks. In *IEEE IGARSS*, July 2018.
- [5] M. H. P. Fuchs and B. Demir. HySpecNet-11k: A large-scale hyperspectral dataset for benchmarking learning-based hyperspectral image compression methods. *arXiv:2306.00385 [cs.CV]*, 2023.
- [6] F. Huang, Y. Yu, and T. Feng. Hyperspectral remote sensing image change detection based on tensor and deep learning. *J. of Vis. Comm. Image Repr.*, 58:233–244, 2019. doi: [10.1016/j.jvcir.2018.11.004](https://doi.org/10.1016/j.jvcir.2018.11.004).
- [7] L. Khelifi and M. Mignotte. Deep Learning for Change Detection in Remote Sensing Images: Comprehensive Review and Meta-Analysis. *IEEE Access*, 8:126385–126400, 2020. doi: [10.1109/ACCESS.2020.3008036](https://doi.org/10.1109/ACCESS.2020.3008036).
- [8] Y. Li et al. A deep learning method for change detection in synthetic aperture radar images. *IEEE TGRS*, 57(8):5751–5763, 2019. doi: [10.1109/TGRS.2019.2901945](https://doi.org/10.1109/TGRS.2019.2901945).
- [9] E. Lopinto et al. Current Status and Future Perspectives of the PRISMA Mission at the Turn of One Year in Operational Usage. In *2021 IGARSS*, pages 1380–1383, 2021. doi: [10.1109/IGARSS47720.2021.9553301](https://doi.org/10.1109/IGARSS47720.2021.9553301).
- [10] J. López-Fandiño et al. Stacked autoencoders for multi-class change detection in hyperspectral images. In *IGARSS 2018*, pages 1906–1909, 2018. doi: [10.1109/IGARSS.2018.8518338](https://doi.org/10.1109/IGARSS.2018.8518338).
- [11] M. W. Malila. Change vector analysis: an approach for detecting forest changes with landsat. *Proc. 6th Ann. Sympos. Mach. Proc. Rem. Sens. Data, Purdue Univ.*, pages 326–335, 1980.
- [12] J. Nieke and M. Rast. Status: Copernicus Hyperspectral Imaging Mission For The Environment (CHIME). In *IGARSS 2019*, pages 4609–4611, 2019. doi: [10.1109/IGARSS.2019.8899807](https://doi.org/10.1109/IGARSS.2019.8899807).
- [13] S.-E. Qian. Hyperspectral Satellites, Evolution, and Development History. *IEEE JSTARS*, 14:7032–7056, 2021. doi: [10.1109/JSTARS.2021.3090256](https://doi.org/10.1109/JSTARS.2021.3090256).
- [14] S. Saha, F. Bovolo, and L. Bruzzone. Unsupervised deep change vector analysis for multiple-change detection in VHR images. *IEEE TGRS*, 57(6):3677–3693, 2019.
- [15] A. Shafique et al. SSViT-HCD: A Spatial Spectral Convolutional Vision Transformer for Hyperspectral Change Detection. *IEEE JSTARS*, pages 1–20, 2023. doi: [10.1109/JSTARS.2023.3251646](https://doi.org/10.1109/JSTARS.2023.3251646).
- [16] A. Singh. Digital change detection techniques using remotely-sensed data. *Int. J. Rem. Sens.*, 10(6):989–1003, 1989. doi: [10.1080/01431168908903939](https://doi.org/10.1080/01431168908903939).
- [17] L. Wang, L. Wan, and L. Bruzzone. A Sub-Pixel Convolution-Based Residual Network for Hyperspectral Image Change Detection. In *IGARSS 2022*, pages 1059–1062, 2022. doi: [10.1109/IGARSS46834.2022.9884805](https://doi.org/10.1109/IGARSS46834.2022.9884805).